

Specialized mechanoreceptor systems in rodent glabrous skin

Jan Walcher¹, Julia Ojeda-Alonso¹, Julia Haseleu¹, Maria K. Oosthuizen², Ashlee H. Rowe³, Nigel C. Bennett² and Gary R. Lewin^{1,4} 

¹Max-Delbrück Centre for Molecular Medicine, Department of Neuroscience, Robert-Rössle Str. 10, 13125, Berlin-Buch, Germany

²Department of Zoology and Entomology, University of Pretoria, Pretoria, Republic of South Africa

³Department of Biology and Program in Cellular and Behavioral Neurobiology, University of Oklahoma, Norman, OK, USA

⁴Excellence Cluster NeuroCure, Charité Universitätsmedizin, 10117, Berlin, Germany

Edited by: Janet Taylor & Diego Contreras

Key points

- An *ex vivo* preparation was developed to record from single sensory fibres innervating the glabrous skin of the mouse forepaw.
- The density of mechanoreceptor innervation of the forepaw glabrous skin was found to be three times higher than that of hindpaw glabrous skin.
- Rapidly adapting mechanoreceptors that innervate Meissner's corpuscles were severalfold more responsive to slowly moving stimuli in the forepaw compared to those innervating hindpaw skin.
- We found a distinct group of small hairs in the centre of the mouse hindpaw glabrous skin that were exclusively innervated by directionally sensitive D-hair receptors.
- The directional sensitivity, but not the end-organ anatomy, were the opposite to D-hair receptors in the hairy skin.
- Glabrous skin hairs in the hindpaw are not ubiquitous in rodents, but occur in African and North American species that diverged more than 65 million years ago.

Abstract Rodents use their forepaws to actively interact with their tactile environment. Studies on the physiology and anatomy of glabrous skin that makes up the majority of the forepaw are almost non-existent in the mouse. Here we developed a preparation to record from single sensory fibres of the forepaw and compared anatomical and physiological receptor properties to those of the hindpaw glabrous and hairy skin. We found that the mouse forepaw skin is equipped with a very high density of mechanoreceptors; >3 times more than hindpaw glabrous skin. In addition, rapidly adapting mechanoreceptors that innervate Meissner's corpuscles of the forepaw were severalfold more sensitive to slowly moving mechanical stimuli compared to their counterparts in the hindpaw glabrous skin. All other mechanoreceptor types as well as myelinated nociceptors

Jan Walcher was born in Starnberg, Germany, in 1982. He studied Biology at the Ludwig-Maximilians-University of Munich and received his diploma degree in 2009, researching sound localization mechanisms of the auditory system. He then worked on the molecular physiology of the somatosensory system at the Max-Delbrück-Centrum in Berlin and received his PhD degree from the Free University of Berlin in 2015. Recently he joined a collaborative research project between the Max-Delbrück-Centrum in Berlin and John Hopkins University in Baltimore investigating molecular similarities of mechanosensation in the auditory and the somatosensory system.



This article was first published as a preprint. Walcher J, Ojeda-Alonso J, Haseleu J, Oosthuizen M, Rowe AH, Bennett NC, Lewin GR. 2018. Specialized mechanoreceptor systems in rodent glabrous skin. bioRxiv. <https://doi.org/10.1101/337923>.

had physiological properties that were invariant regardless of which skin area they occupied. We discovered a novel D-hair receptor innervating a small group of hairs in the middle of the hindpaw glabrous skin in mice. These glabrous skin D-hair receptors were direction sensitive albeit with an orientation sensitivity opposite to that described for hairy skin D-hair receptors. Glabrous skin hairs do not occur in all rodents, but are present in North American and African rodent species that diverged more than 65 million years ago. The function of these specialized hairs is unknown, but they are nevertheless evolutionarily very ancient. Our study reveals novel physiological specializations of mechanoreceptors in the glabrous skin that likely evolved to facilitate tactile exploration.

(Received 5 June 2018; accepted after revision 20 August 2018; first published online 22 August 2018)

Corresponding author G. R. Lewin: Max Delbrück Centre for Molecular Medicine, Robert-Roessle Str. 10, 13125, Berlin-Buch, Germany. Email: glwin@mdc-berlin.de

Introduction

In the past the tactile sense of rodents has been investigated predominantly through the study of hairy skin sensation (Li *et al.* 2011; Lechner & Lewin, 2013; Zimmerman *et al.* 2014). This is despite the fact that many classical behavioural assessments of rodent sensation such as the Hargreaves test (Hargreaves *et al.* 1988) or mechanical withdrawal threshold measurements with von Frey hairs are actually carried out by stimulating the glabrous skin (Ventéo *et al.* 2016; Peng *et al.* 2017; Wetzel *et al.* 2017). In addition, rodents constantly use their forepaws to explore their environment, for example selecting food objects or engaging in grooming behaviour. Indeed such exploratory or active touch tasks uniquely involve the forepaw glabrous skin as the primary sensory surface used. The mouse forepaw is in many respects analogous to the human hand, but has hardly been examined at the functional or anatomical level. A more detailed exploration of glabrous skin sensory receptors in the mouse is even more relevant considering the increasing interest in skilled forelimb movements, tactile feedback during movement and perceptual tasks based on sensory stimuli applied to the forepaw glabrous skin (Fink *et al.* 2014; Milenkovic *et al.* 2014; Estebanez *et al.* 2017; Wetzel *et al.* 2017). Several types of mechanoreceptors have been characterized using electrophysiology mostly in the mouse hairy skin (Koltzenburg *et al.* 1997; Lewin & Moshourab, 2004; Milenkovic *et al.* 2008). One mechanoreceptor type important for tactile sensation is the rapidly adapting mechanoreceptor (RAM) which fires only to skin movement, but innervates morphologically distinct end-organs in hairy skin and glabrous skin (Lewin & Moshourab, 2004; Omerbašić *et al.* 2015). Thus RAMs innervating hairy skin form lanceolate endings around hair follicles, but innervate Meissner's corpuscles in the glabrous skin (Li *et al.* 2011; Heidenreich *et al.* 2012; Wende *et al.* 2012). However, even at the molecular level RAMs in glabrous and hairy skin utilize the same potassium channel, KCNQ4, to regulate their sensitivity to low frequency vibratory stimuli (Heidenreich *et al.*

2012). The functional properties of hairy and glabrous skin RAMs are thought to be similar in humans, but this has not been systematically investigated in rodents.

The primary aim of the present study was to investigate the physiology and anatomy of cutaneous afferents in the mouse forepaw skin. In order to answer the question of whether forepaw afferents differ significantly from those in other skin regions, we also used identical methods to record from hindpaw glabrous and hairy skin receptors. Here we used the *ex vivo* skin nerve method, a well-established technique for studying single sensory receptors in rodents. The most commonly used preparation is that of the saphenous nerve, which innervates the hairy skin of the lateral foot and ankle (Reeh, 1986; Kress *et al.* 1992; Koltzenburg *et al.* 1997). Only a few studies have recorded from sensory receptors in the tibial nerve in rodents, which innervates the hindpaw glabrous skin (Leem *et al.* 1993; Cain *et al.* 2001; Milenkovic *et al.* 2014). Here we developed a novel *ex vivo* skin nerve preparation to record from mouse sensory receptors with axons in the ulnar and median nerves which innervate the forepaw glabrous skin. We compared data using this preparation with recordings from sensory receptors in the tibial and saphenous nerves that innervate hindlimb glabrous and hairy skin, respectively. We show that RAMs that innervate Meissner's corpuscles in the forepaw skin are much more sensitive to low frequency vibration stimuli and are also present at a much higher density than those in other skin areas. Myelinated nociceptors had physiological properties that were invariant across skin areas. We also discovered a novel D-hair receptor population innervating a distinct group of very small hairs only found within the hindlimb glabrous skin. These glabrous hair receptors are not ubiquitous in rodents, but do occur in rodent species from North America and Africa that diverged more than 65 million years ago (Fabre *et al.* 2012). Thus our study reveals unique features of both forepaw and hindpaw glabrous skin receptors that are highly relevant for tactile driven behaviour.

Methods

Ethical approval

All regulated procedures carried out on animals involved in this publication were applied for and approved by the Landesamt für Gesundheit und Soziales (LAGeSo, State of Berlin) and were in full compliance with German and EU animal protection laws. Tissues for physiological and anatomical experiments were obtained from animals that were killed humanely by cervical dislocation or by exposure to a rising concentration of CO₂ gas. Before and throughout the experiments, mice were maintained in plastic cages with commercial bedding, tap water, commercial pelleted diet freely provided and kept in rooms with a 12 h light–dark cycle. Additional institutional animal care and use committee approval was obtained for anaesthetizing southern grasshopper mice for the purpose of photographing hindpaw glabrous skin hairs (Michigan State University IACUC). The investigators understand the ethical principles under which *The Journal of Physiology* operates and state that this work complies with these principles.

Ex vivo skin–nerve preparations

Electrophysiological recordings from fibres of the saphenous nerve were made using an *ex vivo* skin nerve preparation as previously described (Koltzenburg *et al.* 1997; Milenkovic *et al.* 2008) with some minor modifications. The animal was sacrificed by cervical dislocation and the hairs of the limb were shaved off. The hairy skin of the upper leg was carefully removed and the saphenous nerve was dissected up to the hip and cut. The paw skin with the connected nerve was transferred into a bath chamber and fixed with insect needles using the outside-out configuration (Fig. 1C). The bath chamber was constantly perfused with warm (32°C) oxygen-saturated synthetic interstitial fluid. The nerve end was passed through a narrow channel into an adjacent recording chamber that was filled with mineral oil. Since the outside-out configuration was used, a 1 ml pipette was used to regularly flush the dermis of the skin sample with fresh synthetic interstitial fluid buffer.

For the tibial nerve *ex vivo* skin nerve preparation, the hairy skin of the hindpaw was removed, the bones detached, and any remaining muscle and ligament tissue was carefully dissected (Milenkovic *et al.* 2014). We noticed that remaining muscles or ligaments around the nerve trunks decreased the time in which the preparation could be used and often interfered with mechanical and electrical stimulation procedures. Therefore, as much muscle and tendon tissue as possible was removed. A clean preparation (Fig. 1D) allowed for several hours of recordings with reliable mechanical and electrical stimulation using

the outside-out configuration with bath conditions as described above.

For the forepaw *ex vivo* skin nerve preparation, we removed the hairy skin of the forepaw, the bones, ligaments and muscle tissue instead of stripping the glabrous skin from the forepaw. Due to the challenging anatomy around the thenar and hypothenar pads, some remaining muscle tissue was not dissected. Using the outside-out configuration (Fig. 1I) these preparations allowed for high quality recordings of several hours even though the total experimental times were shorter compared to experiments using the hindpaw preparations described above (approximately 2–3 h shorter).

Single-unit recordings were made as previously described (Koltzenburg *et al.* 1997; Milenkovic *et al.* 2008, 2014). Fine forceps were used to remove the perineurium of the nerve. Fine nerve bundles were teased and attached to a platinum wire that served as the recording electrode. Mechanical sensitive units were first located using blunt stimuli applied with a glass rod. The spike pattern and the sensitivity to stimulus velocity were used to classify the unit, as previously described (Milenkovic *et al.* 2008; Ranade *et al.* 2014). A Powerlab 4/30 system and Labchart 7.1 software with the spikes-histogram extension (ADInstruments Ltd., Dunedin, New Zealand) were used to record the raw data. The conduction velocity was measured from the latency between the electrical stimulus and arrival of the action potential at the electrode. All mechanical responses analysed were corrected for this time delay. The total distance that the action potentials travelled could be measured by taking the distance between the stimulation electrode (receptor site) and the recording electrode (nerve end). The conduction velocity (CV) could be measured using the formula $CV = \text{distance}/\text{time delay}$, in which CVs $> 10 \text{ m s}^{-1}$ were classified as $A\beta$, $< 10 \text{ m s}^{-1}$ as $A\delta$ and $< 1.0 \text{ m s}^{-1}$ as C-fibres.

Mechanical stimulation of receptor units were performed using a piezo actuator (Physik Instrumente, Karlsruhe, Germany, P-841.60; see Fig. 2A) and a double-ended Nanomotor (Kleindiek Nanotechnik, Reutlingen, Germany, MM-NM3108) connected to a force measurement device (Kleindiek Nanotechnik, Reutlingen, Germany, PL-FMS-LS). A magnetic stand connected to a micromanipulator assisted in the positioning of the piezo actuator. As the different receptor units are tuned to specific stimuli, different mechanical stimuli were used based on the unit type: a vibrating stimulus with increasing amplitude (using the piezo actuator) was used with a vibration frequency of 20 Hz (Fig. 2B). The force needed to evoke the first action potential was measured. Only the low threshold mechanoreceptors were tested with this stimulus. A dynamic mechanical stimulus with a ramp and hold waveform was used with a constant force (using the piezo actuator; average force of 100 mN) and repeated with varying probe movement velocity (0.075, 0.15, 0.45

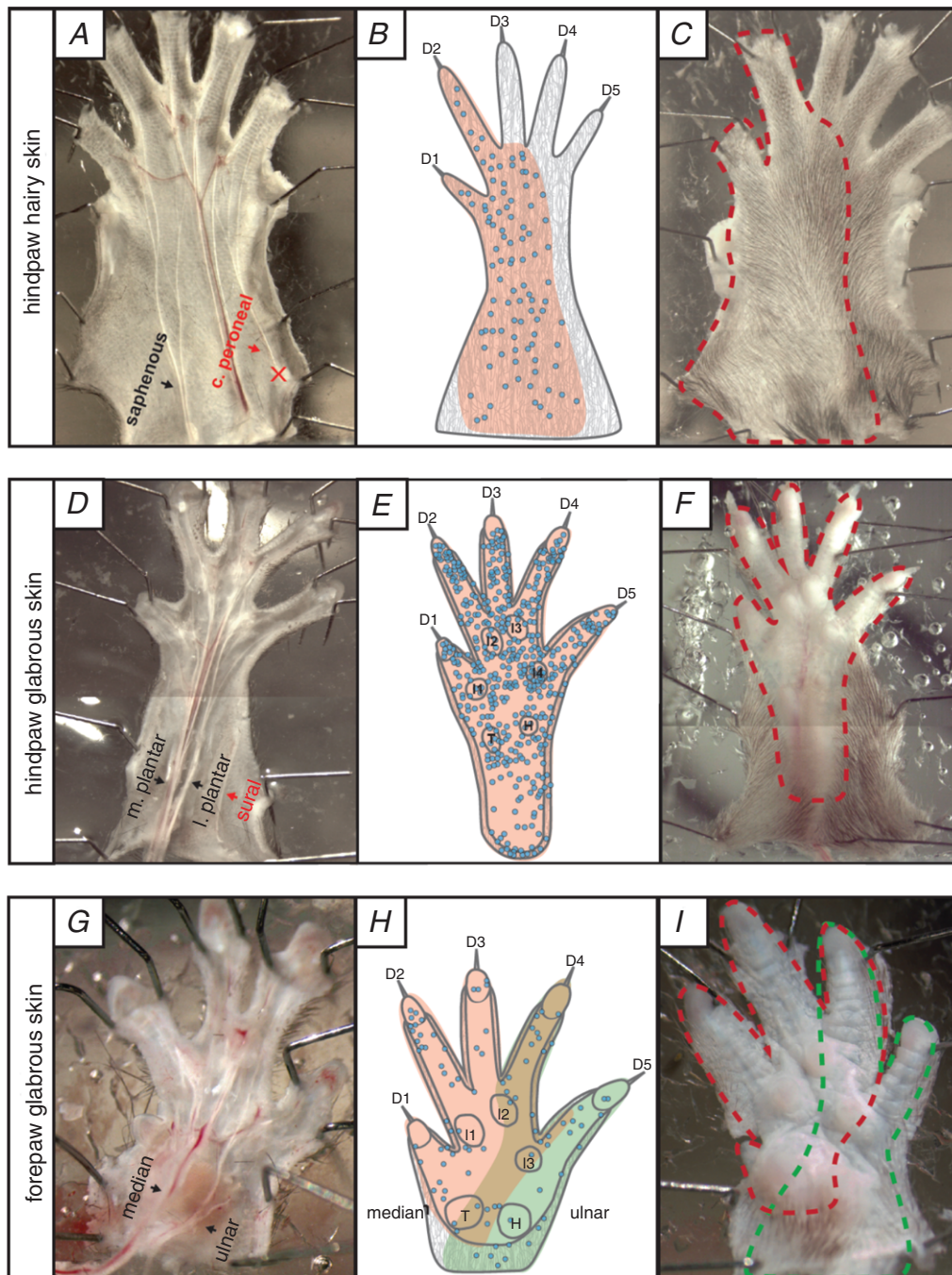


Figure 1. Innervation areas of the saphenous, tibial and median/ulnar nerves

Left: inside out configuration of the hindpaw hairy skin (A), the hindpaw glabrous skin (D) and the forepaw glabrous skin (G) preparation. Nerves indicated in red were not used and the location of the cut end is marked 'X'. Middle: receptor locations of single units recorded from the saphenous nerve (B), the medial and lateral plantar nerve (E), which are two branches of the tibial nerve, and the median (red area) and ulnar nerves (green area) (H) are indicated as well as the skin territory with an overlapping innervation (brown). Blue circles indicate single-unit receptive field centres (compiled data from the current study, data recorded earlier (Milenkovic *et al.* 2014) and unpublished experiments). D, digits; H, hypothenar pads; I, interdigital pads; T, thenar pads. Right: outside-out configuration used in electrophysiological experiments (illustrated as mirror images). Dotted lines indicate the receptive fields of the saphenous nerve (C), the lateral and medial plantar nerve (F) and the median and ulnar nerve (I).

and 1.5 mm s^{-1}). Only the spikes of the dynamic phase were analysed, and only low threshold mechanoreceptors were tested with this stimulus (see Fig. 2C). A static mechanical stimulus with a ramp and hold waveform was used with a constant fast ramp ($1.5\text{--}2 \text{ mN ms}^{-1}$) and repeated with varying amplitude (using the double-ended Nanomotor). Only spikes evoked during the static phase were analysed (Fig. 2D). This stimulus was only used to investigate slowly adapting mechanoreceptors (SAMs) and $A\delta$ -mechanonociceptors (AMs). For single hair stimulation, to selectively move single hairs a fine glass

capillary (tip size approximately $150 \mu\text{m}$) attached to a micromanipulator (Kleindiek Nanotechnik, MM3A) was used. Single hairs could be mounted inside the capillary (Fig. 5E) and then displaced into two-dimensional space using a step protocol (8-, 16-, 32-, 64- and 128-course steps, frequency of $3200 \text{ steps s}^{-1}$, step size approximately $6.3 \mu\text{m}$ – this slightly varied depending on the angle, total length of the axis and distance to the skin). The action potentials triggered during the probe movement were quantified. Images and videos were visualized and captured using a stereomicroscope with a camera

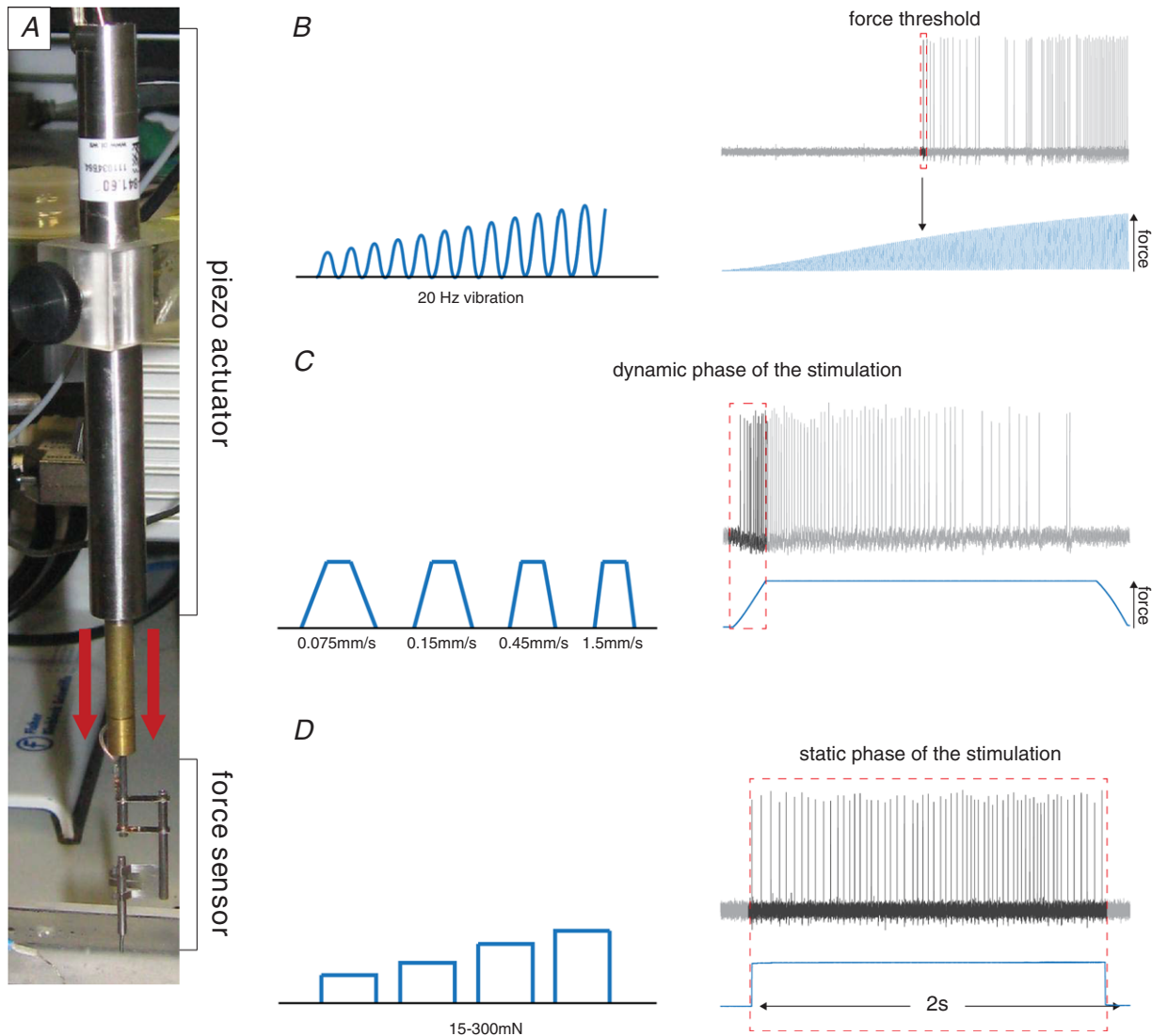


Figure 2. Stimulation protocols

A, example image of the stimulation motor (piezo actuator, Physik Instrumente) and the force feedback system (force sensor, Kleindiek Nanotechnik). B, left, schematic illustration of the sigmoidal vibrating stimulus (20 Hz) with increasing intensity. Right, example trace of a receptor fibre responding to the vibrating stimulus. The force at the time of the first action potential was measured. C, left, schematic illustration of the ramp and hold stimulation; four different velocities were used. Right, example trace of a receptor fibre responding to a ramp and hold stimulation; only the spikes at the dynamic phase of the stimulation were measured. D, left, schematic illustration of the ramp and hold stimulation; four different intensities were used. Right, example trace of a receptor fibre responding to a ramp and hold stimulation; only the spikes during the static phase of the stimulation were quantified.

attached (Leica Microsystems, Wetzlar, Germany, MS5, IC80, LAS software). The video signal of both screens displaying the camera signal and the electrophysiological responses were simultaneously recorded (DebugMode, Wink, TM 2.0 build 1060, freeware, available at <http://www.debugmode.com/wink/>) and saved as single video frames.

Immunofluorescence and anatomy

Skin tissue was dissected removing the hypodermis, ligaments and muscle tissue and stretched out using insect pins. The samples were then fixed at room temperature for 45–60 min in 4% paraformaldehyde. For whole-mount staining the samples were bleached at 4°C for 24 h in 10% H₂O₂, 18% dimethyl sulfoxide–72% methanol, washed five times with methanol and post-fixed at 4°C for 24 h in 20% dimethyl sulfoxide–80% methanol.

Four- to six-week-old heterozygous Cav3.2Cre mice were anaesthetized by an intraperitoneal injection of ketamine (100 mg kg⁻¹) and xylazine (10 mg kg⁻¹). The sciatic or saphenous nerve were exposed and 2 µl of AAV-flex-tdTomato (AV2/9.CAG.FLEX.tdTomato.WPRE.bGH; Penn Vector Core, Philadelphia, PA, USA) with a titre of 3.71×10^{12} was slowly injected into the nerve using a pulled glass capillary attached to a Hamilton microlitre syringe. After the injection, the capillary was left in place for an additional 3 min. The wound was closed with sterile sutures and the animals monitored carefully until they were awake and healthy. All treated animals recovered well and were kept in the animal house and given free access to food and water for 8 weeks before being sacrificed for the final experiments. Treated animals were monitored daily and no adverse effects of the surgery were noted.

For gelatin vibrating blade microtome sections, the tissues were placed into disposable embedding moulds (Polysciences, Warrington, PA, USA, T-8) filled with warm (45°C) 20% gelatin dissolved in phosphate-buffered saline (PBS) and positioned for sagittal sectioning until curing. The gelatin block was post-fixed at 4°C ON in 4% paraformaldehyde and cut in PBS into 120 µm-thick slices using a vibrating blade microtome (Leica Biosystems, Wetzlar, Germany, VT100S).

Tissue clearing

The skin samples were washed in PBS and incubated at 4°C for 1 h with blocking solution (PBS + 5% goat or donkey serum and 0.4% Triton X-100 (Sigma-Aldrich, St Louis, MO, USA)). Primary antibodies were incubated for 48 h at 4°C in blocking solution. After thorough washing with PBS, the secondary antibodies diluted in blocking solution were incubated for 24 h.

Samples were washed in PBS and incubated each time at 4°C for 12 h in a mix of 1:1 PBS–H₂O and a rising concentration of 2,2'-thiodiethanol (TDE; Sigma-Aldrich, St Louis, MO, USA). TDE concentrations were increased from 10% to 25%, 50% and 97%, at which the samples were stored and mounted onto slides and coverslips (remaining in a 97% TDE solution).

Antibody staining

Antibodies used were rabbit anti-S100 (Dako, Carpinteria, CA, USA) cat. no. Z0311, RRID:AB_10013383 diluted 1:1000; chicken anti-NF200 (Millipore (Billerica, MA, USA) cat. no. AB5539, RRID:AB_177520 diluted 1:1000; anti-rabbit Alexa Fluor 488 (Thermo Fisher Scientific, Waltham, MA, USA, cat. no. A-11008, RRID:AB_143165) diluted 1:800; and anti-chicken Alexa Fluor 647 (Thermo Fisher Scientific, Waltham, MA, USA, cat. no. A-21449, RRID:AB_2535866) diluted 1:800.

Image acquisition and analysis

Tiled image stacks were taken using confocal microscopes (Carl Zeiss, Oberkochen, Germany, LSM 700 and LSM710) running Zen 2009 software. Nerve fibre innervation of Meissner's corpuscles was visualized and counted using Fiji/ImageJ with the Bio-Formats extension (Fiji/ImageJ 1.51w National Institutes of Health, USA). Only nerve fibres labelled for both S100 and NF200 were counted. The volume of single Meissner's corpuscle and the volume between the basement membrane and the dermis of each stack were estimated using the integrated area tool of Fiji/ImageJ multiplied by the stack thickness (usually 2 µm). Total volume was calculated by the sum of the corresponding stack volumes.

Electron microscopy

Saphenous, tibial, median and ulnar nerves were dissected and fixed in 4% paraformaldehyde and 2.5% glutaraldehyde in phosphate buffer, post-fixed and contrasted with osmium tetroxide and embedded in Technovit 7100 resin (Heraeus Kulzer, Wehrheim, Germany). Myelinated nerve fibres were quantified using thin toluidine blue-stained 1 µm semi-thin sections (Fig. 4G).

Origin of American and African rodent species

The collection of *Oncyhomys torridus* (southern grasshopper mouse), *Peromyscus leucopus* (white-footed deer mouse) and *Neotoma albigula* (white-throated woodrat) was approved by an Arizona scientific collecting permit. *O. torridus*, *P. leucopus* and *N. albigula* were collected from the Sonoran Desert in southern Arizona (Santa Rita Experimental Range). Permits for the capture

and import of African species including region of capture were as follows: *Heliophobius emini* (Emin's mole-rat, Morogoro District, Tanzania, permit from TWIRA National Parks), *Georychus capensis* (Cape mole-rat, Darling, Cape Town, permit from western Cape Nature Conservation), *Bathyergus suillus* (Cape dune mole-rat, Darling, Cape Town, permit from western Cape Nature conservation), *Cryptomys hottentotus mahali* (Mahali mole-rat, Patryshoek, Gauteng, permit from Gauteng Nature Conservation), *Cryptomys hottentotus pretoriae* (Highveld mole-rat, Tygerpoort, Gauteng, permit from Gauteng Nature Conservation) and *Fukomys damarensis* (Damaraland mole-rat, Hotazel, Northern Cape, permit from northern Cape Nature Conservation), *Otomys sloggetti* (ice rat, Rhodes area, Eastern Cape, permit from Eastern Cape Nature Conservation), *Micaelamys namaquensis* (Namaqua rock mouse, Ezemvelo, Gauteng, permit from Gauteng Nature Conservation), *Saccostomys campestris* (South African pouched mouse, Van Zylsrus area, Northern Cape, permit from Northern Cape Nature Conservation) and *Rhabdomys dilectus* (four striped grass rat, Rietvlei, Gauteng, permit from Gauteng Nature Conservation).

Photography of North American and African rodent feet

We obtained photographs of the hindpaw skin from different rodent species, in some cases from living captive species that were lightly restrained including *Heliophobius emini* (Emin's mole-rat), *Georychus capensis* (Cape mole-rat), *Bathyergus suillus* (Cape dune mole-rat), *Cryptomys hottentotus mahali* (Mahali mole-rat), *Cryptomys hottentotus pretoriae* (Highveld mole-rat), *Fukomys damarensis* (Damaraland mole-rat), *Otomys sloggetti* (ice rat), *Micaelamys namaquensis* (Namaqua rock mouse) and *Saccostomys campestris* (South African pouched mouse). In other cases photographs were taken from post-mortem specimens that had been sacrificed for another unrelated purpose including *Peromyscus leucopus* (white-footed deermouse), *Heterocephalus glaber* (naked mole-rat), *Neotoma albigula* (white-throated woodrat) and *Rhabdomys dilectus* (four striped grass rat). Photographs of the hindpaw of *O. torridus* were taken from lightly anaesthetized animals (through inhaled isoflurane).

Additional software used

Carl-Zeiss Zen 2009 v2.3 lite, Fiji/ImageJ and Adobe creative suite v5.5 were used for Image, video and figure arrangement and processing. Raw data were stored and processed using Microsoft Excel. Statistical tests were performed using Prism 5 and 6 (GraphPad Software, San Diego, CA, USA).

Results

Comparative study of sensory afferents innervating forepaw and hindpaw

We directly compared the functional properties of identified mechanoreceptors and myelinated nociceptors across three skin areas of the mouse. We used an established *ex vivo* preparation for the hindpaw hairy and glabrous skin innervated by the saphenous and tibial nerves, respectively (Koltzenburg *et al.* 1997; Milenkovic *et al.* 2008, 2014) (Fig. 1A–F). In addition, we established a new *ex vivo* preparation that enabled us to record from the median and ulnar nerves that predominantly innervate the mouse forepaw glabrous skin (see Methods and Fig. 1G–I). We used teased nerve fibre recordings to record from single units with myelinated axons and characterized their receptor properties in detail. We took a comparative approach using identical methodologies to record from and characterize the receptor properties of all myelinated afferents forming endings in the hindpaw and forepaw skin. In total, we made recordings from 111 A β -fibres (conduction velocities >10 m s⁻¹) and 92 A δ -fibres (conduction velocities between 1.0 and 10 m s⁻¹) (data summarized in Table 1). Single-unit data were obtained from 52 male and female mice aged between 5 and 8 weeks.

The receptive fields of myelinated axons were localized throughout the saphenous nerve territory (Fig. 1B); no receptive fields of saphenous nerve afferents were found to innervate adjacent glabrous skin (Fig. 1A–C). In our previous study we chiefly recorded from thinly myelinated polymodal nociceptors with axons in the tibial nerve innervating the hindpaw glabrous skin (Milenkovic *et al.* 2014). Here we focused our analysis on afferents with myelinated axons that project to the glabrous skin via the lateral and medial plantar nerves that can be seen in the inside-out version of the *ex vivo* preparation (Fig. 1D). Receptive fields were found throughout the hindpaw glabrous skin, but axons within the tibial nerve that project to the digits at the hairy–glabrous transition zone also sometimes innervated hairs (Fig. 1D–F). We routinely cut the sural nerve that contains some axons that innervate a thin sliver of glabrous skin on the lateral edge of the foot (Smith *et al.* 2013).

We developed a novel preparation that allowed us to make recordings from myelinated sensory afferents innervating the forepaw glabrous skin. The forepaw glabrous skin is innervated by the median and ulnar nerves. Recordings from skin regions with afferents in either nerve revealed that the functional nerve territories show some overlap in the middle of the paw. For example, digit 4 was innervated by afferents from both the median and ulnar nerves. As in the hindpaw, the majority of axons within the median and ulnar nerves formed a

Table 1. Conduction velocities of recorded primary afferents

Type	Hindpaw hairy skin (saphenous nerve)	Hindpaw glabrous skin (tibial nerve)	Forepaw glabrous skin (median/ulnar nerve)
Aβ-fibres			
Count (<i>n</i>)	36	36	39
Conduction velocity (m s ⁻¹)	14.45 ± 0.70	13.69 ± 0.54	13.55 ± 0.54
RAM			
Count (<i>n</i>)	14	14	21
Conduction velocity (m s ⁻¹)	12.75 ± 1.01	13.90 ± 1.01	13.21 ± 0.82
<i>P</i> (one-way ANOVA)		0.6894	
SAM			
Count (<i>n</i>)	22	22	18
Conduction velocity (m s ⁻¹)	15.63 ± 0.89	13.56 ± 0.61	13.71 ± 0.87
<i>P</i> (one-way ANOVA)		0.1195	
Aδ-fibres			
Count (<i>n</i>)	24	42	26
Conduction velocity (m s ⁻¹)	6.24 ± 0.47	7.13 ± 0.46	6.65 ± 0.59
D-hair			
Count (<i>n</i>)	10	18	8
Conduction velocity (m s ⁻¹)	4.78 ± 0.35	7.04 ± 0.46	6.36 ± 0.98
<i>P</i> (one-way ANOVA)		0.0308	
Bonferroni's multiple comparison test			
<i>P</i> (saph. vs. tibial)	<0.05	<0.05	—
Saph. vs. median/ulnar	n.s.	—	n.s.
Tibial vs. median/ulnar	—	n.s.	n.s.
AM			
Count (<i>n</i>)	14	24	18
Conduction velocity (m s ⁻¹)	7.33 ± 0.61	7.20 ± 0.76	6.78 ± 0.75
<i>P</i> (one-way ANOVA)		0.8775	

AM, A δ -mechanonociceptor; n.s., non-significant; RAM, rapidly adapting mechanoreceptor; SAM, slowly adapting mechanoreceptor.

receptive field within the glabrous skin, but hairy skin at the border of the glabrous skin (e.g. at the wrist or digits) was occasionally innervated by these axons (Fig. 1G–I). We noted that it was extremely important to remove muscle tissue surrounding the nerve branches in both the forepaw and hindpaw glabrous skin preparations in order to maintain tissue viability. In the best cases, recordings could be made for up to 8 h following tissue removal. Note that all recordings in this study were made with the skin in the outside-out configuration (illustrated in Fig. 1C, F and I), and thus stimuli were delivered to the skin surface as would be the case *in vivo*.

Receptor properties of A β -fibre and A δ -fibre afferents across skin regions

Each single receptor unit could be classified according to conduction velocity and stimulus response properties as one of four types of mechanoreceptor (Table 1). To apply quantitative mechanical stimuli to the receptive field, we used a piezo-driven actuator equipped with a force measurement device (Fig. 2A). This set-up

allowed us to apply vibration stimuli of different frequencies with increasing amplitude, a protocol that allows the determination of force threshold for activation of mechanoreceptors. An example of such a determination for a rapidly adapting mechanoreceptor (RAM) that responds to a 20 Hz vibration is shown in Fig. 2B. We also used ramp and hold stimuli in which the 2 s-long static phase was suprathreshold to activate the receptor, and the velocity of the ramp was varied to probe the dynamic (or velocity) sensitivity of the receptor (Fig. 2C). Analysis of spike rates only during the ramp phase of the stimuli was used to assess the velocity sensitivity of the receptor. The example shown in Fig. 2C is from a slowly adapting mechanoreceptor (SAM) which fires at much higher rates during the dynamic phase of the stimulus compared to the static phase. This stimulus protocol was applied to all afferent types that show dynamic responses to moving stimuli, i.e. RAMs, SAMs and D-hair receptors (Heidenreich *et al.* 2012; Lechner & Lewin, 2013; Zimmerman *et al.* 2014). Most nociceptors do not respond to skin movement but rather code static intensity. In this study we recorded the mechanosensitivity

of SAMs and A δ -fibres with nociceptor properties (so called A δ -mechanonociceptors; AMs) across different skin regions. The receptor properties of these fibres were probed with a series of ramp and hold stimuli of constant velocity in which the amplitude was increased incrementally from 15 to 300 mN (Fig. 2D).

Rapidly adapting mechanoreceptors

RAMs respond exclusively to moving stimuli, rapidly ceasing to fire after cessation of movement (Fig. 3A). Most RAMs in the hairy skin are associated with hair follicles, while the RAMs of the glabrous skin are associated with Meissner's corpuscles (Heidenreich *et al.* 2012; Lechner & Lewin, 2013; Zimmerman *et al.* 2014; Poole *et al.* 2014b). Forty-nine of the 111 A β -fibres recorded could be classified as RAMs and these receptors were equally sampled across hindpaw hairy skin, hindpaw glabrous skin and forepaw skin (Table 1). We used increasing

amplitude vibration stimuli to assess the mean force threshold to activate all RAMs that innervate the different skin regions. The mean force thresholds were, as expected, very low with thresholds <3 mN. There was a tendency for forepaw afferents (median and ulnar nerve) to be activated with smaller forces compared to afferents in hairy skin (saphenous nerve) or those innervating the hindpaw glabrous skin (tibial nerve), but this difference was not statistically significant (Fig. 3B; saphenous: $n = 13$; tibial: $n = 13$; median/ulnar: $n = 21$; Kruskal—Wallis test, $P = 0.6476$).

There was a quantitatively large difference in the way that RAMs in the glabrous forepaw skin coded moving stimuli compared to RAMs innervating hairy skin (Fig. 3C). Forepaw RAMs responded reliably with high firing rates to the slowest ramps used (0.075 and 0.15 mm s⁻¹), whereas hairy skin RAMs barely responded to the same stimuli (Fig. 3A and C) and these differences were statistically significant (saphenous:

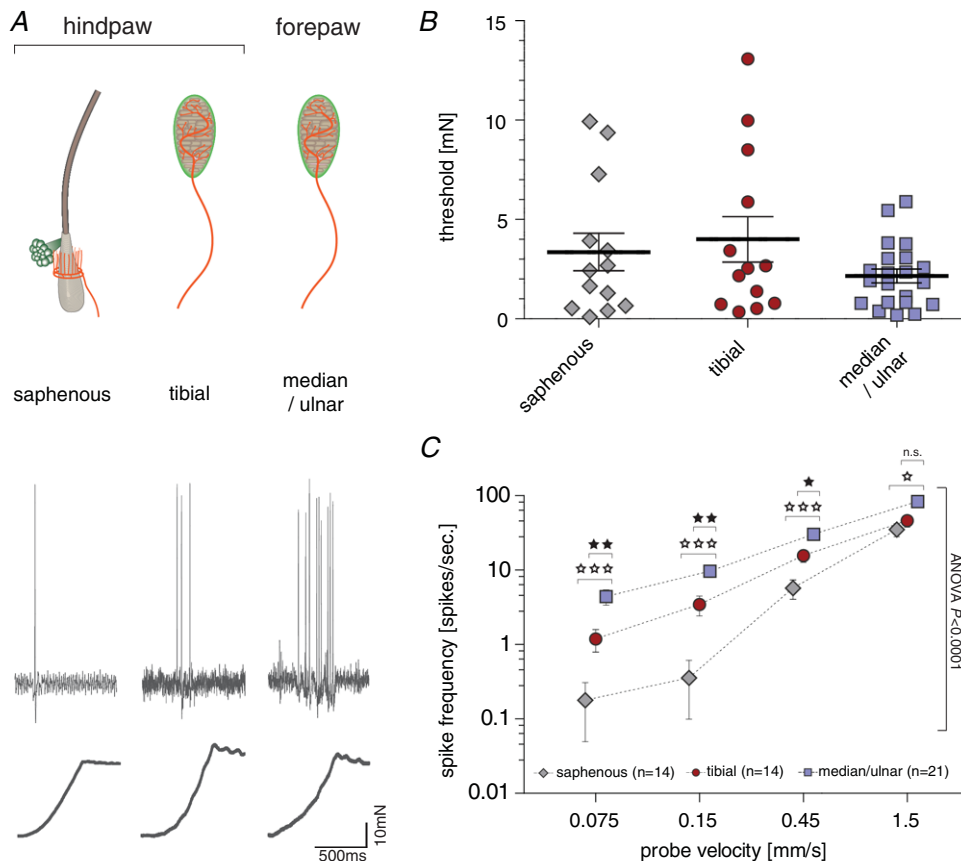


Figure 3. Response properties of RAMs
 A, top, schematic drawing of the predominant RAM anatomy in saphenous nerve preparation (hair follicle receptor), tibial nerve preparation (Meissner's corpuscle) and median/ulnar nerve preparation (Meissner's corpuscle). Bottom, representative example traces of RAMs in response to a ramp and hold stimulation with a velocity of 0.45 mm s⁻¹.
 B, minimal stimulation force needed to evoke an action potential in response to increasing amplitude vibrating stimuli (20 Hz); ANOVA: $P > 0.05$; error bars represent SEM.
 C, average spike frequency in response to moving stimuli. Repeated measures ANOVA: $P < 0.0001$; Bonferroni *post hoc* tests are indicated; *** $P < 0.001$, ** $P < 0.01$, * $P < 0.05$; error bars represent SEM.

$n = 14$; tibial: $n = 14$; median/ulnar: $n = 21$; repeated measures ANOVA, $F(2, 46) = 15.22$, $P < 0.0001$). Thus RAMs in the forepaw glabrous skin are tuned to slower movements, but also have firing rates that were severalfold higher than observed for afferents innervating hairy skin (Fig. 3A and C; ANOVA with Bonferroni *post hoc* test, $P < 0.0001$; 0.075 mm s^{-1} (saphenous *vs.* median/ulnar), $P < 0.001$; 0.15 mm s^{-1} (saphenous *vs.* median/ulnar), $P < 0.001$; 0.45 mm s^{-1} (saphenous *vs.* median/ulnar), $P < 0.05$). The vast majority of the forepaw RAMs had receptive fields clearly located in the glabrous skin and therefore likely innervate Meissner's corpuscles. It is possible that a very small number of receptors innervated hair follicles on the glabrous-hairy skin border, but due to the receptive field distributions (Fig. 1) these afferents could not make up more than 10% of the total. The majority of RAMs in the tibial nerve also innervate glabrous skin and therefore also likely have Meissner's corpuscle endings. However, the sensitivity of RAMs found in the glabrous hindpaw skin did not match that of the forepaw RAMs (Fig. 3A and C; ANOVA with Bonferroni *post hoc* test: tibial *vs.* median/ulnar 0.075 mm s^{-1} , $P < 0.01$; 0.15 mm s^{-1} , $P < 0.01$; 0.45 mm s^{-1} , $P < 0.05$; 1.5 mm s^{-1} , $P > 0.05$). Glabrous hindpaw RAMs were, however, capable of encoding slower velocities than RAMs in hairy skin, but this was not statistically significant (Fig. 3C).

Because presumptive Meissner's corpuscle receptors located in the glabrous forepaw were more responsive to ramp stimuli than those in the hindpaw, we questioned whether receptor morphology differed between these two locations. In the first step we investigated the number of nerve fibres associated with each Meissner's corpuscle. We used immunofluorescence methods to visualize Meissner's corpuscles and their innervation in hindpaw and forepaw glabrous skin. We used antibodies against S100 which is found in terminal Schwann cells that form the corpuscle and antibodies against NF200 to visualize the myelinated axons that innervate the corpuscle (Fig. 4A and B). We examined a total of 175 Meissner's corpuscles (84 located in the hindpaw glabrous skin and 91 located in the forepaw glabrous skin) and counted the number of myelinated nerve fibres innervating each corpuscle (Fig. 4D). Evidently each corpuscle in the forepaw skin was on average innervated by more axons than those in the hindpaw. Thus, more than 50% of corpuscles were found with two to three innervating axons in the forepaw whereas in the hindpaw 70% of the corpuscles were innervated by one to two axons only (Fig. 4C; hindpaw: median = 2, mean = 2.02 ± 0.09 fibres, $n = 84$; forepaw: median = 3, mean = 2.57 ± 0.91 fibres, $n = 91$; mean \pm SEM; Mann-Whitney *U* test, $P < 0.0001$). It could be that the increased innervation of Meissner's corpuscles in the forepaw is simply due to larger corpuscles in this skin area.

However, we measured the volume (V) of 135 Meissner's corpuscles (65 from hindpaw and 70 from forepaw skin) and found that there was no difference in their mean volumes (Fig. 4D; hindpaw: $V = 3.53 \times 10^3 \mu\text{m}^3$, $n = 65$; forepaw: $V = 3.52 \times 10^3 \mu\text{m}^3$, $n = 70$; mean \pm SEM; Mann-Whitney *U* test, $P = 0.6645$). We next measured the overall density of Meissner's corpuscles in the forepaw and hindpaw glabrous skin. Using confocal microscopy we could image a large volume of skin and measure precisely the number of corpuscles in a known volume (see Supplementary Video 1). We chose to image the elevated interdigital pads of the glabrous paw skin, sometimes called 'running pads' (indicated in Fig. 1E, F, H and I), as these are discrete and easily identifiable regions that can be directly compared between fore- and hindpaw skin. We measured the average number of Meissner's corpuscles per volume (μm^3) of skin (Fig. 4B, top) within the interdigital pads III closest to the second digit of the forepaw or the corresponding interdigital pad IV of the hindpaw ($n = 7$ animals, age = P23–28). On average 34.6 ± 2.7 Meissner's corpuscles in the forepaw and 43.3 ± 3.4 Meissner's corpuscles in the hindpaw were counted within one interdigital pad. Thus, the average density of Meissner's corpuscles was significantly higher in the forepaw glabrous skin interdigital pad III with 1.10 ± 0.09 corpuscle per $10^{-6} \mu\text{m}^3$ compared to interdigital pad IV of the hindpaw with 0.81 ± 0.03 corpuscles per $10^{-6} \mu\text{m}^3$ (Fig. 4E; paired *t* test: $P = 0.0188$).

We used semi-thin sections of peripheral nerves to make quantitative estimates of the total number of myelinated fibres in the tibial nerve that innervate the hindpaw glabrous skin compared to the number of myelinated fibres in median and ulnar nerves that innervate the forepaw glabrous skin. The mean myelinated axon count for the median and ulnar nerves combined was 1723 ± 56 ($n = 3$) compared to 1422 ± 4 ($n = 3$) for the entire tibial nerve (Fig. 4F). We estimated the innervated area of the hindpaw glabrous skin innervated by the tibial nerve to be 2.9 larger than the innervated area of the forepaw glabrous skin innervated by the median and ulnar nerves (median/ulnar: 65 ± 2.2 fibres mm^{-2} ; tibial: 22 ± 0.4 fibres mm^{-2} , 4 animals age P23–28; mean \pm SEM). Therefore, it is obvious that the forepaw glabrous skin has as much as a threefold higher afferent innervation density in terms of myelinated fibres compared to the hindpaw glabrous skin.

Slowly adapting mechanoreceptors

Slowly adapting type mechanoreceptors respond well to both indentation and vibration stimuli. To compare SAMs in hairy skin to those with receptive fields in glabrous skin, a ramp and hold stimulus was used. The response of a typical SAM is shown in Fig. 5A. Of the 111 A β -fibres recorded across all skin areas, 62 were SAMs: 22 from the hindpaw hairy skin, 22 from the hindpaw glabrous

skin and 18 from the forepaw glabrous skin. We calculated the mean firing rate of all SAMs to suprathreshold ramp and hold stimuli (2 s long) over time by binning spike counts into 100 ms bins (Fig. 5B). As expected, mean firing rates were highest during the dynamic phase (up to 150 Hz) and adapted to lower rates during the static phase (5–15 Hz). Importantly, no significant differences in the spike rates were found for SAMs recorded across the three skin regions (Fig. 5B; saphenous: $n = 20$; tibial: $n = 20$; median/ulnar: $n = 18$; repeated measures ANOVA, $F(2, 55) = 1.20$; $P = 0.3087$). We also used a series of increasing ramp velocities with constant suprathreshold force to probe SAM velocity sensitivity as described above for RAMs (Fig. 5C). The stimulus response functions

were typical for SAMs and the velocity sensitivities of the receptors were almost identical across the three skin regions tested (Fig. 5C; saphenous: $n = 21$; tibial: $n = 22$; median/ulnar: $n = 16$; repeated measures ANOVA, $F(2, 56) = 1.11$; $P = 0.3364$). We next tested the sensitivity of the SAMs to static indentation using a series of stimuli varying from 15 up to 250 mN. The mean rates of firing reached a plateau around 60 mN for SAM receptors across all three skin regions confirming that these receptors are tuned to detect low intensity threshold static indentation (Fig. 5D). Across the saphenous nerve (hindpaw hairy skin), the tibial nerve (hindpaw glabrous skin) and the median/ulnar nerve (forepaw glabrous skin) there was no statistically significant difference in the mean stimulus

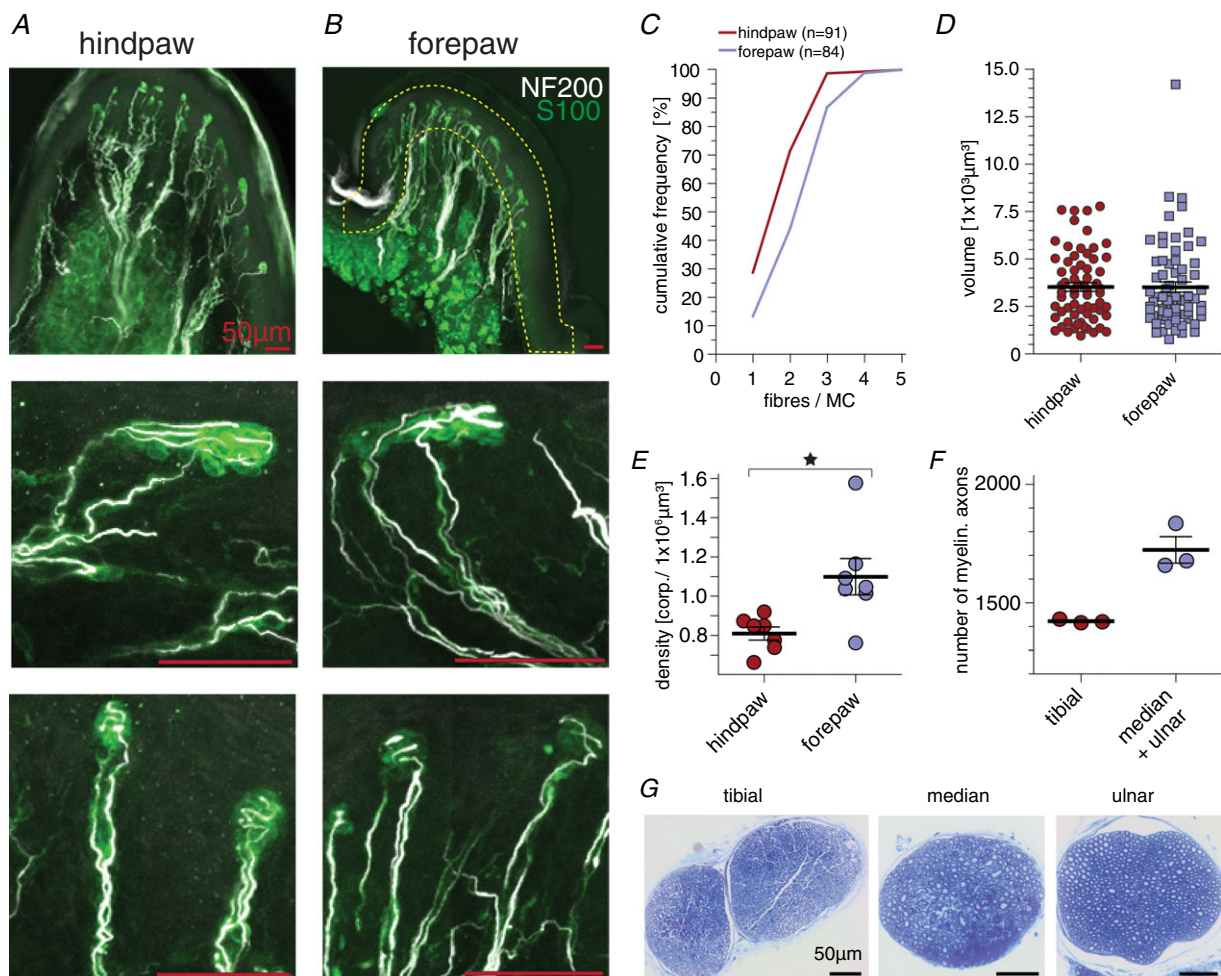


Figure 4. Meissner's corpuscle anatomy

A and B, sagittal vibrating blade microtome sections of the interdigital pad IV of the hindpaw (A) and the interdigital pad III of the forepaw (B). Top, immunofluorescence image of a running pads with labelled Meissner's corpuscle (anti-S100) and myelinated nerve fibres (anti-NF200). Middle and bottom, magnified representation of single Meissner's corpuscles. C, cumulative frequency plot of the number of fibres innervating a single Meissner's corpuscle. D, size (volume) of Meissner's corpuscle in the hind- and forepaw running pads; error bars represent SEM. E, Meissner's corpuscle density in the interdigital running pads III (hindpaw) and IV (forepaw); paired t test: $P = 0.0188$; error bars represent SEM. F, number of myelinated axons counted in the tibial and the median plus the ulnar nerve; error bars represent SEM. G, representative semi-thin microscopy images used to quantify myelinated axon number. All scale bars in panels A and B are 50 μm .

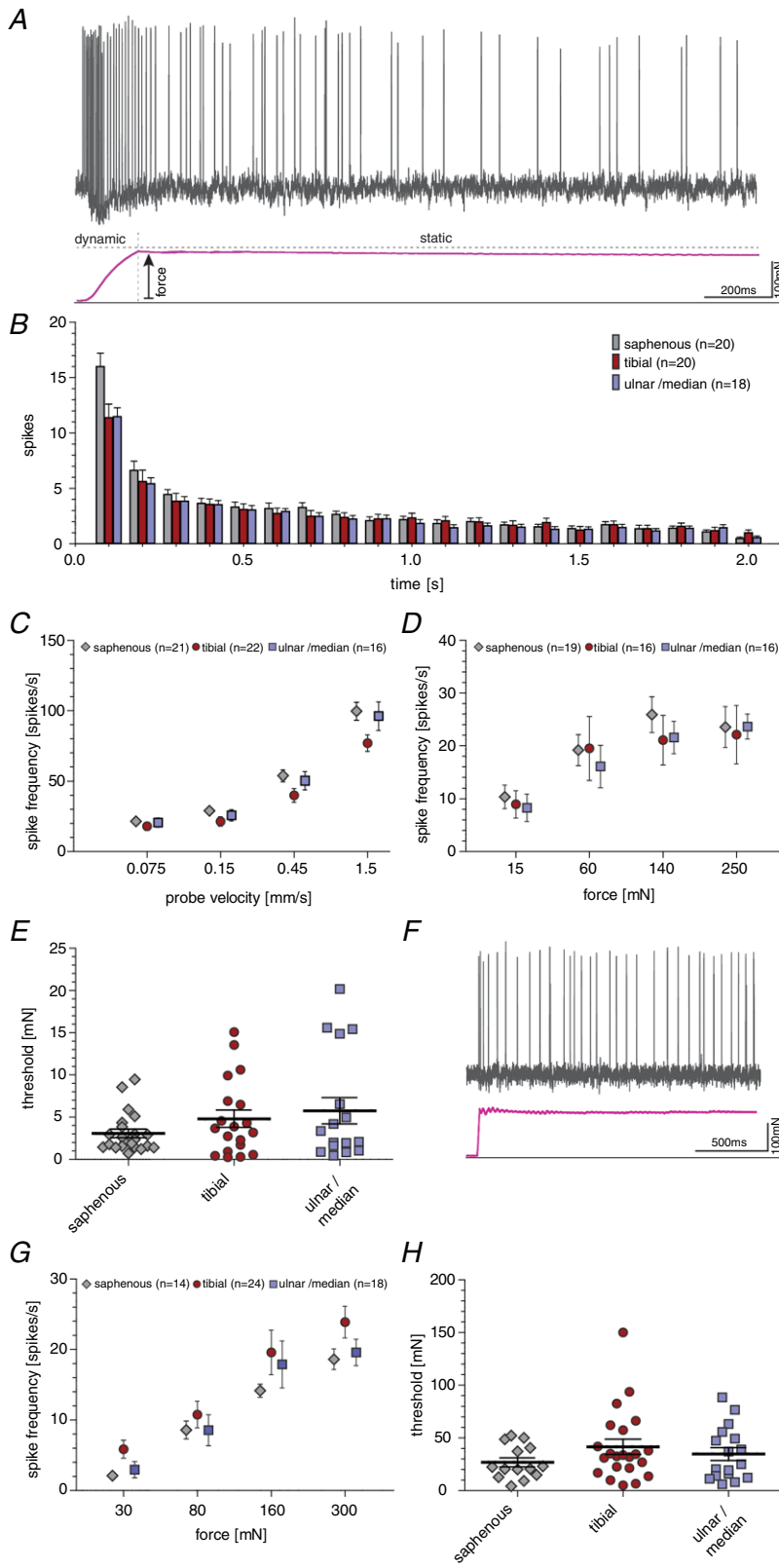


Figure 5. Receptor properties of SAMs

A, representative example trace of a SAM response (hindpaw glabrous skin) to a ramp and hold stimulation. **B**, average spike count (bin 0.1 s) to a suprathreshold mechanical stimulus over 2 s duration. **C**, average spike frequency of SAMs in response to moving stimuli; repeated measures ANOVA: $P > 0.05$; error bars represent SEM. **D**, average spike frequency of SAMs in response to ramp and hold stimulation; repeated measures ANOVA: $P > 0.05$; error bars represent SEM. **E**, minimal force needed to evoke an action potential of SAMs in response to 20 Hz vibrating stimuli; repeated measures ANOVA: $P > 0.05$; error bars represent SEM. **F**, representative example trace of an AM response (hindpaw glabrous skin) to a ramp and hold stimulation. **G**, average spike frequency of AMs in response to ramp and hold stimulations; repeated measures ANOVA: $P > 0.05$; error bars represent SEM. **H**, minimal force needed to evoke an action potential in AMs in response to a fast moving ramp stimulation; repeated measures ANOVA: $P > 0.05$; error bars represent SEM.

response for the static component between SAMs (Fig. 5D; saphenous: $n = 19$; tibial: $n = 16$; median/ulnar: $n = 16$; repeated measures ANOVA, $F(2, 48) = 0.23$; $P = 0.7923$). Finally, we estimated the force threshold for SAMs using a 20 Hz vibration stimulus. As expected, most SAMs had very low thresholds for activation (mostly between 1 and 5 mN) and the mean thresholds were not statistically significantly different from each other across the three skin regions (Fig. 5E; saphenous: $n = 22$; tibial: $n = 19$; median/ulnar: $n = 17$; Kruskal–Wallis test, $P = 0.6444$). By analysing the variance of firing rates during static indentation it is possible to distinguish between SAM type I receptors innervating Merkel cells and SAM type II receptors that do not innervate Merkel cells (Wellnitz *et al.* 2010). Analysing our data set using this method revealed no differences in the proportion of SAM type I and SAM type II receptors across skin regions. In addition, the receptor properties of both SAM types were not different across the three skin regions (data not shown).

A δ -fibre mechanonociceptors

Myelinated nociceptors, also called A δ -mechanonociceptors (Lewin & Moshourab, 2004), are thought not to be associated with specific structures or corpuscles in the skin (Kruger *et al.* 1981; Arcourt *et al.* 2017). Myelinated nociceptors have been extensively studied in the hairy skin and typically respond with increasing firing rates to increasing static force (Garell *et al.* 1996; Lewin & Moshourab, 2004; Milenkovic *et al.* 2008). A total of 56 AMs were studied: 14 with a receptive field in hindpaw hairy skin, 24 with a receptive field in hindpaw glabrous skin and 18 with receptive fields in forepaw glabrous skin. Stimulus response functions to steadily increasing ramp and hold stimuli with intensities ranging from 30 to 300 mN were plotted (Fig. 5F and G). The stimulus response functions of AMs found in all three skin areas were indistinguishable from each other and there was no statistically significant difference between them (Fig. 5G; saphenous: $n = 14$; tibial: $n = 24$; median/ulnar: $n = 18$; repeated measures ANOVA, $F(2, 53) = 2.15$; $P = 0.1262$). For each AM unit we also measured the minimum force necessary to trigger the first action potential and again noted that in each skin area comparable high mechanical thresholds were found (Fig. 5H). Mean thresholds were slightly higher in the two glabrous skin areas, but this was not significantly different (Kruskal–Wallis test; saphenous: $n = 14$; tibial: $n = 22$; median/ulnar: $n = 17$; $P = 0.4887$). Thus, the mechanosensitive properties of A δ -mechanonociceptors appear to be uniform across different skin areas.

D-hair receptors

D-hairs are the most sensitive mechanoreceptors in the skin and generally have the largest receptive fields (Burgess

et al. 1968; Lewin & McMahon, 1991; Leem *et al.* 1993; Koltzenburg *et al.* 1997; Wang & Lewin, 2011; Lechner & Lewin, 2013). A total of 36 D-hair receptors were recorded: 10 from the hindpaw hairy skin (saphenous nerve), 18 from the hindpaw glabrous skin (tibial nerve) and eight from the forepaw glabrous skin (median and ulnar nerves) (Table 1). All recorded D-hair receptors had conduction velocities in the A δ -fibre range (between 1 and 10 m s⁻¹); however, the mean conduction velocities of D-hair receptors in nerves innervating glabrous skin (tibial, median and ulnar nerves) were significantly faster than those recorded in the saphenous nerve that exclusively innervates hairy skin (Table 1). We used the same protocols to test velocity sensitivity of D-hair receptors as we had used for RAMs. D-hair receptors are especially sensitive to fast moving stimuli (Fig. 6A and B) and had very low mechanical thresholds to vibration stimuli (Fig. 6C). There was no significant difference in the mean mechanical thresholds of D-hair receptors recorded across the three skin areas (Fig. 6C; saphenous: $n = 13$; tibial: $n = 10$; median/ulnar: $n = 5$; Kruskal–Wallis test, $P = 0.41$). Importantly, the coding properties of all D-hair receptors recorded were almost identical across all three skin areas (Fig. 6B and C; saphenous: $n = 10$; tibial: $n = 18$; median/ulnar: $n = 7$; repeated measures ANOVA, $F(2, 32) = 1.50$; $P = 0.24$).

We recorded many D-hair receptors with axons in the tibial nerve; some of these afferents had receptive fields in the hairy skin at the transition zones between glabrous and hairy skin at the heel and toes. However, we discovered a group of very fine hairs (~20–30 in total) in the central region of the glabrous skin surrounded by the so-called running pads in all mice examined (Fig. 6D). Around half of the D-hair receptors recorded from the tibial nerve had a receptive field in this area and were specifically activated by movements of these very fine hairs. We rarely found classical RAMs that could be clearly activated by movement of the same set of hairs. When we observed such units it was impossible to determine if the movement of the hair was actually activating Meissner receptor endings in the near vicinity. These observations led us to hypothesize that these glabrous hindpaw hairs are almost exclusively innervated by D-hair receptors.

Recently, it was shown that D-hair receptors in the back skin show direction sensitivity (Rutlin *et al.* 2014). The hairs in the middle of the hindpaw glabrous skin are unusual in that the space between individual hairs is so large that it is straightforward to move a single hair without any danger of simultaneously manipulating adjacent hairs (Fig. 6E). We used a glass capillary to capture a single hair and by using a stepping motor we were able to move the hair in two-dimensional space (see Supplementary Video 2). As shown in Fig. 6D, all these very fine hairs lie flat on the skin with hair growth orientated towards the toes. Placing the hair within the capillary meant that adjustment

to a central position led to transient activation of the D-hair receptor, but firing ceased as soon as movement stopped. We then moved the hairs in the direction of growth, bending the hair in the direction of the toes, which led to the most robust activation of the receptor. In contrast, movement of the hair against its growth led to a weaker activation of the receptor. Thus, we were able to quantify the directional sensitivity of these receptors (Fig. 6F, Table 2 and Supplementary Video 2). Movement of the hair from side to side generally led to an intermediate level of receptor activation (Table 2). The directional sensitivity of these specialized D-hair receptors means that their

activation is greatest when the hairs are pushed against the skin. Therefore, under normal circumstances these receptors would be best activated as the animal places its foot on a surface. Activation would be least if the foot slides over a rough surface in the direction of forward movement.

We took advantage of the fact that, in the adult, expression of the T-type calcium channel $Ca_v3.2$ gene is highly specific for D-hair receptors (Shin *et al.* 2003; Wang & Lewin, 2011; Bernal Sierra *et al.* 2017). By using a $Ca_v3.2^{Cre}$ mouse combined with adeno-associated virus transduction of sensory axons with AAV9 vectors carrying

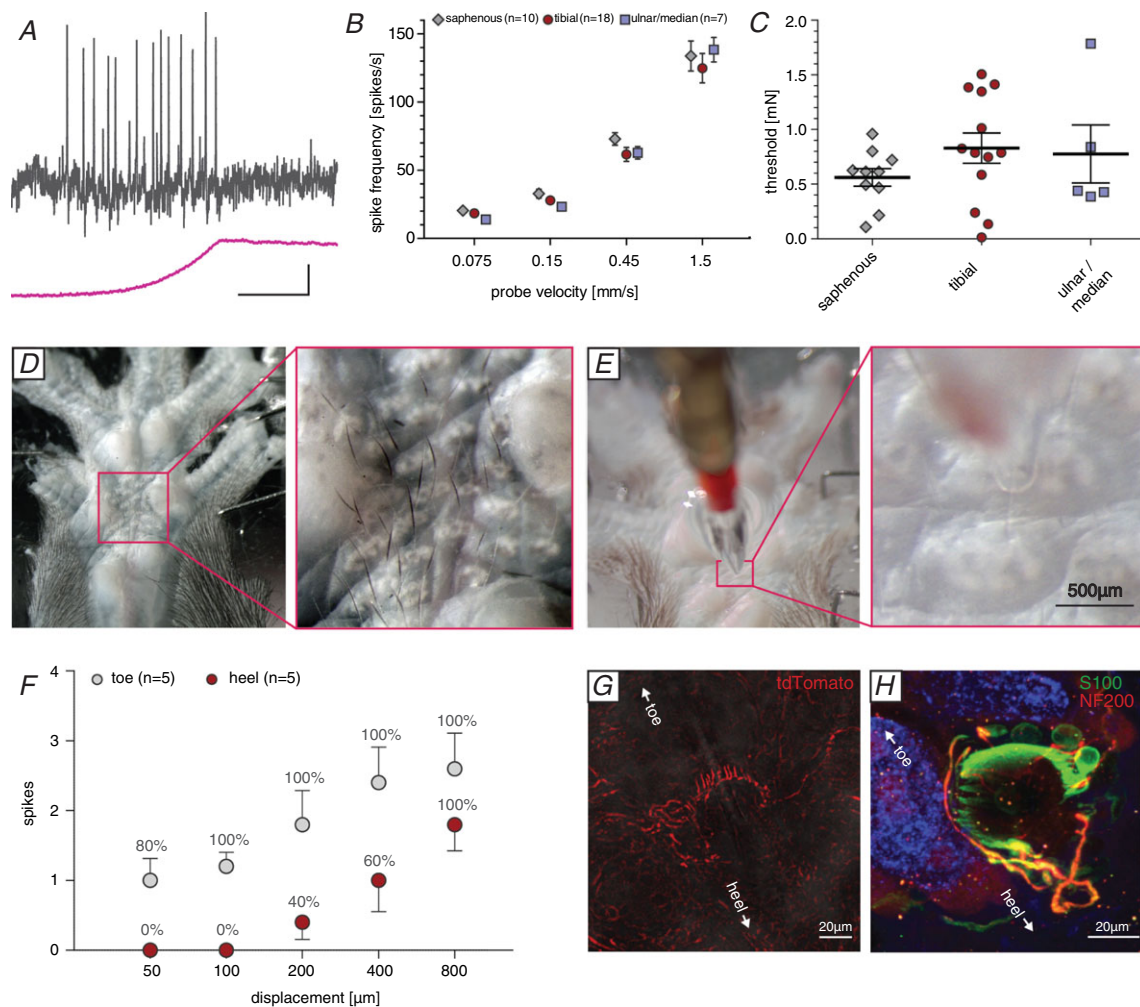


Figure 6. Functional and anatomical properties of glabrous skin D-Hair receptors

A, representative example traces from D-hair receptor recordings in response to a ramp and hold stimulation with a velocity of 0.45 mm s^{-1} . B, average spike frequency in response to moving stimuli. Repeated measures ANOVA: $P > 0.05$; error bars represent SEM. C, minimal stimulation force needed to evoke an action potential in response to increasing vibrating stimuli (20 Hz); ANOVA: $P > 0.05$; error bars represent SEM. D, hairs at the glabrous hindpaw skin. Right panel, magnification. E, experimental set-up of the hair deflection experiment: the mounted hair can be deflected in the direction towards the toe, the heel or sideways. Right panel, magnification to display the hair partially inside the glass capillary. F, D-hair receptors respond with more action potentials (average spikes) and respond more reliable (percentage of receptors responding) to small hair deflections in the direction towards the toe compared to the direction of the heel. Error bars represent SEM. G, $Ca_v3.2$ positive nerve fibres cluster at one side of the follicle (whole-mount preparation). H, whole-mount hair follicle receptor staining; terminal Schwann cells in green (anti-S100), myelinated nerve fibres in red (anti-NF200) and autofluorescence in blue.

Table 2. Responses of glabrous skin D-hairs to hair deflection

Movement direction	Number of steps				
	8	16	32	64	128
Towards the toes					
Responding receptors	4/5	5/5	5/5	5/5	5/5
Mean number of spikes	1	1.2	1.8	2.4	2.6
Towards the heel					
Responding receptors	0/5	0/5	2/5	3/5	5/5
Mean number of spikes	0	0	0.4	1	1.8
Towards the sides*					
Responding receptors	1/5	1/5	2.5/5	5/5	4.5/5
Mean number of spikes	0.2	0.2	0.6	1.3	2.9

*Average of both sides.

a floxed tdTomato reporter, we could specifically label the peripheral terminals of sensory neurons that express the $Ca_v3.2$ gene (Bernal Sierra *et al.* 2017). D-hair receptors form lanceolate endings around hair follicles that, unlike RAMs, do not form a closed circle around the follicle but instead display a horseshoe configuration in which one region of the follicle is devoid of endings (Rutlin *et al.* 2014; Bernal Sierra *et al.* 2017). We injected the adeno-associated AAV9-FLEX-tdTomato virus into the sciatic nerve of $Ca_v3.2^{Cre}$ mice and harvested glabrous skin tissue from the same mice 8 weeks later. We found that in each of the four mice studied we could visualize lanceolate endings around single hair follicles in the glabrous skin (see Supplementary Video 3). D-hair lanceolate endings showed an asymmetrical innervation of the hair follicles so that the open part of the horseshoe was orientated toward the heel (Fig. 6G). In most preparations only a few follicles received a tdTomato-positive innervation consistent with the idea that the viral approach produces sparse labelling. We observed that single D-hair receptors were activated by movements of up to nine of the hairs present, consistent with the idea that single afferents are labelled with the viral labelling approach. Using whole-mount immunostaining in wild-type mice we could visualize the innervation of these hair follicle receptors using primary antibodies against NF200, a marker for myelinated fibres, and S100, staining terminal Schwann cells (Fig. 6H). Immunofluorescence staining using S100 and NF200 antibodies confirmed that these hairs are innervated by myelinated hair follicle receptors that display lanceolate endings (Fig. 6H). In addition, we did observe some circumferential endings around these hairs (Fig. 6H).

Glabrous D-hair receptors are evolutionarily ancient in rodents

The specialized hairs of the glabrous hindpaw skin are likely exclusively innervated by D-hair receptors in laboratory mice. We never observed such hairs on the

forepaw glabrous skin in mice. This raised the question as to whether such hairs, termed here glabrous skin hairs, may have arisen as a non-essential sensory trait through generations of inbreeding in laboratory mice. We used C57BL/6J mice in this study, but we also observed glabrous skin hairs in another inbred mouse strain, CBA/J mice (Carter *et al.* 1952) (Fig. 7A and B). However, there was no evidence of glabrous skin hairs in inbred laboratory rats (*Rattus rattus*, Sprague–Dawley strain) (Fig. 7C).

With over 2000 living species (~40% of all mammals) that populate most continents, rodents are highly successful and diverse (Wilson & Reeder, 2005). We reasoned that glabrous D-hairs may have been an ancient adaptation in this order that has appeared and reappeared during species diversification. We screened the hind feet of three North American rodents in the family Cricetidae and nine African rodent species for the presence of glabrous skin hairs that could be innervated by D-hair receptors. Two of the North American species, *Peromyscus leucopus* (white-footed deer mouse) and *Oncyhomys torridus* (southern grasshopper mouse), had obvious small hairs within the same region of hindpaw glabrous skin as seen in the mouse (Fig. 7D and E). The white-footed deer mouse is distributed across the mid-western and eastern USA (Delaney & Hoekstra, 2018) whereas the southern Grasshopper mouse is restricted to the deserts and grasslands of the western USA and northern Mexico. The white-footed deer mouse is an opportunistic insectivore, while the southern grasshopper mouse, unusually, is an obligate carnivorous rodent that feeds on insects and scorpions (Rowe *et al.* 2013; Rowe & Rowe, 2015). The third North American rodent species, *Neotoma albigula* (white-throated woodrat), clearly lacked hindpaw glabrous hairs (Fig. 8). This species is, like *Oncyhomys torridus*, also found in the dry woodlands and deserts of the southwestern USA and northern Mexico (Spencer & Spencer, 1941).

Among the African rodent species that we surveyed, none of the surface dwelling species, like *Otomys*

sloggetti (ice rat), *Micaelamys namaquensis* (Namaqua rock mouse), *Saccostomys campestris* (South African pouched mouse) and *Rhabdomys dilectus* (four striped grass rat) possessed glabrous skin hairs (Fig. 8). There is a rich diversity of exclusively underground living African mole-rat species from the family *Bathyergidae* found from the Horn of Africa to the Cape region in South Africa. We surveyed the glabrous hindpaws of seven African mole-rats, *Heterocephalus glaber* (naked mole-rat), *Heliophobius emini* (Emin's mole-rat), *Georchus capensis* (Cape mole-rat), *Bathyergus suillus* (Cape dune mole-rat), *Cryptomys hottentotus mahali* (Mahali mole-rat), *Cryptomys hottentotus pretoriae* (Highveld mole-rat) and *Fukomys damarensis* (Damaraland mole-rat), with at least one representative species from each of the six genera of *Bathyergidae* examined. One of these species, *Fukomys damarensis*, a eusocial species found in southwestern and central Africa (Bennett & Jarvis, 1988; Bennett & Faulkes, 2000; Davies *et al.* 2015), possessed discrete groups of glabrous skin hairs with remarkably similar morphology to those of the laboratory mouse (Fig. 7E). As in the laboratory mouse,

small hairs within the glabrous skin of the forepaw were never observed in the other rodent species.

Discussion

Here we show that it is possible to record from mouse forepaw afferents using a novel *ex vivo* skin nerve preparation. By comparing the physiological properties of sensory afferents across three skin areas, we identified novel specializations of mouse forepaw glabrous skin receptors. Firstly, RAMs that innervate Meissner's corpuscles are severalfold more sensitive to slow skin movement compared to the same receptors in hindpaw glabrous skin, or functionally similar RAMs in hairy skin. Second, individual Meissner's corpuscles are innervated by ~25% more sensory axons than in other skin areas and are present at significantly higher densities in the forepaw compared to hindpaw glabrous skin. Strikingly, all mechanoreceptors with myelinated axons are present at much higher density (>3-fold higher) in the forepaw skin compared to hindpaw glabrous skin. Nevertheless, by recording from all subpopulations



Figure 7. Glabrous skin hair receptors are found in North American and African rodent species

A–F, representative pictures of the glabrous hindpaw skin from laboratory rodents (top row) and three wild caught rodent species from Africa and North America. A and B, images of these very fine hairs in two laboratory inbred mouse strains, C57BL/6J (A) and CBA/J (B) mice. C, we observed no hairs on the glabrous skin of laboratory rats. D and E, sparse fine hairs were observed on the hindpaw glabrous skin of the North American white footed mouse (D) and quite dense hairs were found on the same region of the Grasshopper mouse (E), which has its habitat in the Arizona desert. F, very distinctive glabrous hairs were also observed on the glabrous skin of the Damaraland mole-rat.



Figure 8. Rodent species that lack glabrous skin hairs
 A, one North American rodent species that lacks glabrous D-hair receptors. B–K, 10 African rodent species that clearly lack hindpaw glabrous hairs.

of myelinated mechanoreceptors as well as myelinated nociceptors, we could show that it is only RAMs that show functional specialization in the forepaw. In addition, we also identified a unique population of D-hair receptors that provide an almost exclusive innervation to a small set of hairs within the hindpaw glabrous skin of the mouse. These D-hair receptors show prominent directional sensitivity so that they are optimally activated when these very small hairs are pushed against the skin as would happen during a foot fall. Interestingly, these glabrous D-hair receptors are not ubiquitous in other rodent species, but we show that they have likely arisen very early in rodent evolution as we identified one African mole-rat species and two North American rodent species that appear to possess such hairs (from a total of 12 examined).

Our data suggest that the mouse has a highly developed forepaw tactile system adapted to manipulating objects and exploring their texture. The fact that myelinated sensory fibre receptor density was more than 3-fold higher than in the hindlimb would enable much higher discriminative abilities using the forepaw. We calculated that the density of the myelinated sensory innervation was a striking $65 \text{ fibres mm}^{-2}$. Analogously, in humans, tactile discrimination performance is clearly positively correlated with sensory innervation density which is highest on the finger tips and tongue (Johansson & Vallbo, 1979*a,b*; Van Boven & Johnson, 1994). Indeed mechanoreceptor density on the finger tips has been estimated to be $\sim 240 \text{ cm}^{-2}$ (Johansson & Vallbo, 1979*b*). We show here that Meissner's corpuscle density is not only very much higher in forepaw compared to hindpaw glabrous skin, but also that each corpuscle receives around 25% more sensory endings compared to an equivalent corpuscle in the hindpaw (Fig. 4). The anatomical adaptations that we have described in forepaw Meissner's corpuscles might underlie their functional specialization, including increased sensitivity to slower moving mechanical stimuli (Fig. 3). However, it is not clear why higher densities of sensory axons within a Meissner's corpuscle should increase the velocity sensitivity of the sensory unit. Mechanoreceptors including RAMs that innervate Meissner's corpuscles are thought to be equipped with a mechanotransduction apparatus that includes the mechanosensitive ion channel PIEZO2 and its modulator STOML3 (Ranade *et al.* 2014; Poole *et al.* 2014*a*; Wetzel *et al.* 2017). Indeed small molecule inhibition of STOML3 in the mouse forepaw reversibly reduces the ability of the mouse to perceive mechanical stimuli (Wetzel *et al.* 2017). It is known that the expression of mechanoreceptor-specific potassium channels like KCNQ4 modulate the mechanoreceptor response to low frequency sinusoidal stimuli (Heidenreich *et al.* 2012), so it is conceivable that mouse forepaw afferents express a different complement of potassium channels than mechanoreceptors innervating other skin

regions. The high sensitivity of mouse forepaw Meissner's mechanoreceptors suggests that enhanced tactile acuity in the forepaw has been selected for during evolution and may have fitness advantages by allowing mice to more accurately select their dietary intake according to its tactile properties. The physiological and anatomical specialization of forepaw Meissner's corpuscle receptors was all the more remarkable as other mechanoreceptors, such as SAMs and A δ -nociceptors (Fig. 5), showed mechanosensitive properties that were invariant across the skin areas examined. Thus we can be confident that data gathered on such receptors can be compared regardless of the skin area examined. Conversely, it is also clear from our data that RAMs from the forepaw cannot be compared with those recorded from the hindpaw.

D-hair receptors are the most sensitive cutaneous mechanoreceptors and typically have large receptive fields and can be activated by almost all hairs within the receptive field (Brown & Iggo, 1967; Burgess *et al.* 1968; Lewin & McMahon, 1991; Ritter *et al.* 1991). These mechanoreceptors were first described in cat hairy skin and have been described extensively in rodents, but have essentially identical properties in primates and are also found in humans (Perl, 1968; Adriaensen *et al.* 1983). The development of D-hair receptors is controlled by multiple neurotrophic factors. The number of D-hair receptors that develop in the post-natal skin is controlled by nerve growth factor (Ritter *et al.* 1991; Lewin *et al.* 1992) and in the adult animal D-hair receptors require neurotrophin-4 (NT-4) for survival (Stucky *et al.* 1998, 2002). It has long been known that D-hair receptors express high levels of TrkB the main receptor for brain-derived neurotrophic factor (BDNF) and NT-4 (Shin *et al.* 2003; Li *et al.* 2011; Rutlin *et al.* 2014). A novel physiological and anatomical feature of D-hair receptors is that their end-organ consists of an array of lanceolate endings that form a horseshoe around the innervated hair (Rutlin *et al.* 2014; Bernal Sierra *et al.* 2017) and this anatomical arrangement is thought to underpin strong direction sensitivity. Polarized expression of BDNF in the developing follicle is necessary for the asymmetric structure of the lanceolate endings and for direction sensitivity of the receptor. Here we describe a unique population of small hairs in the mouse hindpaw glabrous skin that appear to be predominantly innervated by D-hair receptors (Fig. 6). Immunostaining of these hairs with antibodies against NF-200 revealed lanceolate endings that were indistinguishable from those seen with tdTomato driven by the D-hair-specific marker Cav3.2 gene (Fig. 6*G* and *H*). Thus other types of mechanoreceptor probably do not provide a lanceolate innervation to these hairs. We could confirm that these D-hair receptors are also directionally sensitive being best activated as the hair was moved against the skin (Fig. 6). In the hairy skin of the mouse back, D-hair receptors were described as best activated by movement of the hair in

the rostral direction, which corresponded with the hair shaft pulling away from the lanceolate endings. Caudal movement of the hair would result in the shaft pushing against the main lanceolate array (Rutlin *et al.* 2014). For the D-hair receptors recorded in the glabrous skin, the situation was directly the opposite, and thus the receptors were most sensitive in the direction where the shaft would be pushed against the main lanceolate array (Fig. 6). There is evidence that protein tethers may link transduction channels in sensory neurons to the extracellular matrix (Hu *et al.* 2010; Chiang *et al.* 2011) and such tethers could link lanceolate endings to the hair follicle shaft (Li & Ginty, 2014). It is conceivable that tethers that link the hair shaft and transduction channels in the lanceolate endings are pulled to gate channels in D-hair receptors in the mouse back skin. The opposite directional sensitivity with the same anatomical arrangement in glabrous skin D-hair receptors means that this model should be modified. It is, for example, conceivable that a tether based transduction mechanism is used by both receptors, but it is the precise positioning of the tethers that determines direction sensitivity. It will only be possible to resolve this issue definitively when the molecular identity of the tether and its relationship to the transduction channels is known. Nevertheless, the unique physiological properties of the glabrous skin D-hair receptor suggest that these hairs serve a distinct and specific sensory role in comparison to the hairy skin D-hair receptors. Recently, several reports in mice have suggested that it is D-hair receptors that drive touch-evoked pain under neuropathic conditions (Ventéo *et al.* 2016; Peng *et al.* 2017; Dhandapani *et al.* 2018). Since in neuropathic models behavioural assessments of increased sensitivity to mechanical stimuli are made using von Frey hairs applied to the glabrous skin of the hindpaw, it is likely that glabrous skin D-hair receptors drive neuropathic behaviour. The role of hairy skin D-hair receptors and the glabrous skin D-hair receptors in normal touch behaviour remains unresolved. Experiments in humans have shown that activity in some mechanoreceptor units, e.g. RAMs and SAM type I receptors, are capable of triggering conscious perception of touch (Vallbo, 1981; Ochoa *et al.* 1983; Torebjork *et al.* 1987; Sanchez Panchuelo *et al.* 2016). However, activity in other mechanoreceptors, such as SAM type II receptors, does not appear to trigger conscious touch perception (Ochoa *et al.* 1983). It is thus entirely possible that under normal circumstances activity in D-hair receptors provides sensory input that modulates motor behaviour but does not contribute to tactile perception. We show here that glabrous D-hair receptors are not ubiquitous in rodents, but are probably evolutionarily ancient. The appearance of these receptors in rodent species that diverged more than 65 million years ago (Fabre *et al.* 2012) suggests that there may be a developmental programme leading to their appearance that has been switched on or off during speciation. Rodent

species that may possess glabrous D-hair receptors, such as the grasshopper mouse and the Damaraland mole-rat, occupy totally different habitats and it is not obvious what might have provided selective pressure for the retention of glabrous skin hair receptors.

In summary, we have provided evidence for unique mechanoreceptor specializations in the mouse glabrous skin. Our data provide a solid basis to evaluate how rodents use their glabrous skin surfaces to explore their tactile environment.

References

- Adriaensen H, Gybels J, Handwerker HO & Van Hees J (1983). Response properties of thin myelinated (A δ) fibers in human skin nerves. *J Neurophysiol* **49**, 111–122.
- Arcourt A, Gorham L, Dhandapani R, Prato V, Taberner FJ, Wende H, Gangadharan V, Birchmeier C, Heppenstall PA & Lechner SG (2017). Touch receptor-derived sensory information alleviates acute pain signaling and fine-tunes nociceptive reflex coordination. *Neuron* **93**, 179–193.
- Bennett NC & Faulkes CG (2000). *African Mole Rats: Ecology and Eusociality*. Cambridge University Press, Cambridge.
- Bennett NC & Jarvis JUM (1988). The social structure and reproductive biology of colonies of the mole-rat, *Cryptomys damarensis* (Rodentia, Bathyergidae). *J Mammal* **69**, 293–302.
- Bernal Sierra YA, Haseleu J, Kozlenkov A, Bégay V & Lewin GR (2017). Genetic tracing of Ca v 3.2 T-type calcium channel expression in the peripheral nervous system. *Front Mol Neurosci* **10**, 70.
- Brown AG & Iggo A (1967). A quantitative study of cutaneous receptors and afferent fibres in the cat and rabbit. *J Physiol* **193**, 707–733.
- Burgess PR, Petit D & Warren RM (1968). Receptor types in cat hairy skin supplied by myelinated fibers. *J Neurophysiol* **31**, 833–848.
- Cain DM, Khasabov SG & Simone DA (2001). Response properties of mechanoreceptors and nociceptors in mouse glabrous skin: An in vivo study. *J Neurophysiol* **85**, 1561–1574.
- Carter TC, Dunn LC, Falconer DS, Heston WE, Grüneberg H & Snell GD (1952). Standardized nomenclature for inbred strains of mice. *Cancer Res* **12**, 602–613.
- Chiang L-Y, Poole K, Oliveira BE, Duarte N, Sierra YAB, Bruckner-Tuderman L, Koch M, Hu J & Lewin GR (2011). Laminin-332 coordinates mechanotransduction and growth cone bifurcation in sensory neurons. *Nat Neurosci* **14**, 993–1000.
- Davies KTJ, Bennett NC, Tsagkogeorga G, Rossiter SJ & Faulkes CG (2015). Family wide molecular adaptations to underground life in African mole-rats revealed by phylogenomic analysis. *Mol Biol Evol* **32**, 3089–3107.
- Delaney EK & Hoekstra HE (2018). Sexual imprinting and speciation between two *Peromyscus* species. *Evolution* **72**, 274–287.
- Dhandapani R, Arokiaraj CM, Taberner FJ, Pacifico P, Raja S, Nocchi L, Portulano C, Franciosa F, Maffei M, Hussain AF, de Castro Reis F, Raymond L, Perlas E, Garcovich S, Barth S,

- Johnsson K, Lechner SG & Heppenstall PA (2018). Control of mechanical pain hypersensitivity in mice through ligand-targeted photoablation of TrkB-positive sensory neurons. *Nat Commun* **9**, 1640.
- Wilson DE & Reeder DM (2005). *Mammal Species of the World: A Taxonomic and Geographic Reference*, 3rd edn. John Hopkins University Press, Baltimore. <https://jhupbooks.press.jhu.edu/content/mammal-species-world>.
- Estebanez L, Hoffmann D, Voigt BC & Poulet JFA (2017). Parvalbumin-expressing GABAergic neurons in primary motor cortex signal reaching. *Cell Rep* **20**, 308–318.
- Fabre P-H, Hautier L, Dimitrov D & P Douzery EJ (2012). A glimpse on the pattern of rodent diversification: a phylogenetic approach. *BMC Evol Biol* **12**, 88.
- Fink AJP, Croce KR, Huang ZJ, Abbott LF, Jessell TM & Azim E (2014). Presynaptic inhibition of spinal sensory feedback ensures smooth movement. *Nature* **509**, 43–48.
- Garell PC, McGillis SL & Greenspan JD (1996). Mechanical response properties of nociceptors innervating feline hairy skin. *J Neurophysiol* **75**, 1177–1189.
- Hargreaves K, Dubner R, Brown F, Flores C & Joris J (1988). A new and sensitive method for measuring thermal nociception in cutaneous hyperalgesia. *Pain* **32**, 77–88.
- Heidenreich M, Lechner SG, Vardanyan V, Wetzel C, Cremers CW, De Leenheer EM, Aránguez G, Moreno-Pelayo MÁ, Jentsch TJ & Lewin GR (2012). KCNQ4 K⁺ channels tune mechanoreceptors for normal touch sensation in mouse and man. *Nat Neurosci* **15**, 138–145.
- Hu J, Chiang L-Y, Koch M & Lewin GR (2010). Evidence for a protein tether involved in somatic touch. *EMBO J* **29**, 855–867.
- Johansson RS & Vallbo AB (1979a). Detection of tactile stimuli. Thresholds of afferent units related to psychophysical thresholds in the human hand. *J Physiol* **297**, 405–422.
- Johansson RS & Vallbo AB (1979b). Tactile sensibility in the human hand: relative and absolute densities of four types of mechanoreceptive units in glabrous skin. *J Physiol* **286**, 283–300.
- Koltzenburg M, Stucky CL & Lewin GR (1997). Receptive properties of mouse sensory neurons innervating hairy skin. *J Neurophysiol* **78**, 1841–1850.
- Kress M, Koltzenburg M, Reeh PW & Handwerker HO (1992). Responsiveness and functional attributes of electrically localized terminals of cutaneous C-fibers in vivo and in vitro. *J Neurophysiol* **68**, 581–595.
- Kruger L, Perl ER & Sedivec MJ (1981). Fine structure of myelinated mechanical nociceptor endings in cat hairy skin. *J Comp Neurol* **198**, 137–154.
- Lechner SG & Lewin GR (2013). Hairy sensation. *Physiology* **28**, 142–150.
- Leem JW, Willis WD & Chung JM (1993). Cutaneous sensory receptors in the rat foot. *J Neurophysiol* **69**, 1684–1699.
- Lewin GR, Lisney SJ & Mendell LM (1992). Neonatal anti-NGF treatment reduces the A δ - and C-fibre evoked vasodilator responses in rat skin: evidence that nociceptor afferents mediate antidromic vasodilatation. *Eur J Neurosci* **4**, 1213–1218.
- Lewin GR & McMahon SB (1991). Physiological properties of primary sensory neurons appropriately and inappropriately innervating skeletal muscle in adult rats. *J Neurophysiol* **66**, 1218–1231.
- Lewin GR & Moshourab R (2004). Mechanosensation and pain. *J Neurobiol* **61**, 30–44.
- Li L & Ginty DD (2014). The structure and organization of lanceolate mechanosensory complexes at mouse hair follicles. *Elife* **3**, e01901.
- Li L, Rutlin M, Abraira VE, Cassidy C, Kus L, Gong S, Jankowski MP, Luo W, Heintz N, Koerber HR, Woodbury CJ & Ginty DD (2011). The functional organization of cutaneous low-threshold mechanosensory neurons. *Cell* **147**, 1615–1627.
- Milenkovic N, Wetzel C, Moshourab R & Lewin GR (2008). Speed and temperature dependences of mechanotransduction in afferent fibers recorded from the mouse saphenous nerve. *J Neurophysiol* **100**, 2771–2783.
- Milenkovic N, Zhao W-JW-J, Walcher J, Albert T, Siemens J, Lewin GR & Poulet JF (2014). A somatosensory circuit for cooling perception in mice. *Nat Neurosci* **17**, 1560–1566.
- Ochoa J, Torebjörk E & Torebjörk E (1983). Sensations evoked by intraneural microstimulation of single mechanoreceptor units innervating the human hand. *J Physiol* **342**, 633–654.
- Omerbašić D, Schuhmacher L-N, Bernal Sierra Y-A, Smith ESJ & Lewin GR (2015). ASICs and mammalian mechanoreceptor function. *Neuropharmacology* **94**, 80–86.
- Peng C, Li L, Zhang M-D, Bengtsson Gonzales C, Parisien M, Belfer I, Usoskin D, Abdo H, Furlan A, Häring M, Lallemand F, Harkany T, Diatchenko L, Hökfelt T, Hjerling-Leffler J & Ernfors P (2017). miR-183 cluster scales mechanical pain sensitivity by regulating basal and neuropathic pain genes. *Science* **356**, 1168–1171.
- Perl ER (1968). Myelinated afferent fibres innervating the primate skin and their response to noxious stimuli. *J Physiol* **197**, 593–615.
- Poole K, Herget R, Lapatsina L, Ngo H-D & Lewin GR (2014a). Tuning Piezo ion channels to detect molecular-scale movements relevant for fine touch. *Nat Commun* **5**, 3520.
- Poole K, Moroni M & Lewin GR (2014b). Sensory mechanotransduction at membrane-matrix interfaces. *Pflugers Arch* **467**, 121–132.
- Ranade SS, Woo S-HH, Dubin AE, Moshourab RA, Wetzel C, Petrus M, Mathur J, Bégay V, Coste B, Mainquist J, Wilson AJ, Francisco AG, Reddy K, Qiu Z, Wood JN, Lewin GR & Patapoutian A (2014). Piezo2 is the major transducer of mechanical forces for touch sensation in mice. *Nature* **516**, 121–125.
- Reeh PW (1986). Sensory receptors in mammalian skin in an in vitro preparation. *Neurosci Lett* **66**, 141–146.
- Ritter AM, Lewin GR, Kremer NE & Mendell LM (1991). Requirement for nerve growth factor in the development of myelinated nociceptors in vivo. *Nature* **350**, 500–502.
- Rowe AH & Rowe MP (2015). Predatory grasshopper mice. *Curr Biol* **25**, R1023–R1026.
- Rowe AH, Xiao Y, Rowe MP, Cummins TR & Zakon HH (2013). Voltage-gated sodium channel in grasshopper mice defends against bark scorpion toxin. *Science* **342**, 441–446.

- Rutlin M, Ho C-Y, Abaira VE, Cassidy C, Woodbury CJ & Ginty DD (2014). The cellular and molecular basis of direction selectivity of A δ -LTMRs. *Cell* **159**, 1640–1651.
- Sanchez Panchuelo RM, Ackerley R, Glover PM, Bowtell RW, Wessberg J, Francis ST & McGlone F (2016). Mapping quantal touch using 7 Tesla functional magnetic resonance imaging and single-unit intraneural microstimulation. *Elife* **5**, e12812.
- Shin J-B, Martinez-Salgado C, Heppenstall PA & Lewin GR (2003). A T-type calcium channel required for normal function of a mammalian mechanoreceptor. *Nat Neurosci* **6**, 724–730.
- Smith AK, O'Hara CL & Stucky CL (2013). Mechanical sensitization of cutaneous sensory fibers in the spared nerve injury mouse model. *Mol Pain* **9**, 61.
- Spencer DA & Spencer AL (1941). Food habits of the white-throated wood rat in Arizona. *J Mammal* **22**, 280.
- Stucky CL, DeChiara T, Lindsay RM, Yancopoulos GD & Koltzenburg M (1998). Neurotrophin 4 is required for the survival of a subclass of hair follicle receptors. *J Neurosci* **18**, 7040–7046.
- Stucky CL, Shin J-BB & Lewin GR (2002). Neurotrophin-4: a survival factor for adult sensory neurons. *Curr Biol* **12**, 1401–1404.
- Torebjork HE, Vallbo AB & Ochoa JL (1987). Intraneural microstimulation in man. Its relation to specificity of tactile sensations. *Brain* **110**, 1509–1529.
- Vallbo AB (1981). Sensations evoked from the glabrous skin of the human hand by electrical stimulation of unitary mechanosensitive afferents. *Brain Res* **215**, 359–363.
- Van Boven RW & Johnson KO (1994). The limit of tactile spatial resolution in humans: grating orientation discrimination at the lip, tongue, and finger. *Neurology* **44**, 2361–2366.
- Ventéo S, Laffray S, Wetzel C, Rivat C, Scamps F, Méchaly I, Bauchet L, Raoul C, Bourinet E, Lewin GR, Carroll P & Pattyn A (2016). Fxyd2 regulates A δ - and C-fiber mechanosensitivity and is required for the maintenance of neuropathic pain. *Sci Rep* **6**, 36407.
- Wang R & Lewin GR (2011). The Ca_v3.2 T-type calcium channel regulates temporal coding in mouse mechanoreceptors. *J Physiol* **589**, 2229–2243.
- Wellnitz SA, Lesniak DR, Gerling GJ & Lumpkin EA (2010). The regularity of sustained firing reveals two populations of slowly adapting touch receptors in mouse hairy skin. *J Neurophysiol* **103**, 3378–3388.
- Wende H, Lechner SG, Cheret C, Bourane S, Kolanczyk ME, Pattyn A, Reuter K, Munier FL, Carroll P, Lewin GR & Birchmeier C (2012). The transcription factor c-Maf controls touch receptor development and function. *Science* **335**, 1373–1376.
- Wetzel C, Pifferi S, Picci C, Gök C, Hoffmann D, Bali KK, Lampe A, Lapatsina L, Fleischer R, Smith ES, Bégay V, Moroni M, Estebanez L, Kühnemund J, Walcher J, Specker E, Neuenschwander M, von Kries JP, Haucke V, Kuner R, Poulet JF, Schmoranzner J, Poole K & Lewin GR (2017). Small-molecule inhibition of STOML3 oligomerization reverses pathological mechanical hypersensitivity. *Nat Neurosci* **20**, 209–218.
- Zimmerman A, Bai L & Ginty DD (2014). The gentle touch receptors of mammalian skin. *Science* **346**, 950–954.

Additional information

Competing interests

The authors declare no competing interests.

Author contributions

J.W. carried out electrophysiology experiments, anatomical experiments, established the forepaw preparation and carried out data analysis. J.O.-A. helped in the acquisition and analysis of skin and nerve anatomy. J.H. performed genetic labelling experiments with AAV vectors and image analysis. M.K.O. and N.C.B. acquired and analysed material from African rodent species and provided interpretation of the data. A.H.R. acquired and analysed material from North American rodent species and provided interpretation of the data. N.C.B. provided analysis and interpretation of the data from African rodent species. G.R.L. helped in acquisition of images from African mole-rats, supervised data analysis, and wrote the paper with intellectual input from all authors. All authors have read and approved the final version of this manuscript and agree to be accountable for all aspects of the work in ensuring that questions related to the accuracy or integrity of any part of the work are appropriately investigated and resolved. All persons designated as authors qualify for authorship, and all those who qualify for authorship are listed.

Funding

This work was supported by grants from the Deutsche Forschungsgemeinschaft (SFB 665 Project B6 to G.R.L.) and a European Research Council advanced grant (ERC 294678).

Acknowledgements

We thank Alison Barker for her comments on the manuscript. We also acknowledge the technical assistance of the Advanced Light Microscopy technology platform of the MDC.

Translational perspective

Rodents such as rats and mice are commonly used as models for disease in humans. The sensory apparatus that underlies our sense of touch is highly conserved between mice and humans. Humans manipulate objects primarily with their hands using non-hairy glabrous skin to investigate the tactile properties of things. Analogous to the human hand, rodents use their forepaws to manipulate objects. For the first time we investigated the sensory innervation of the mouse forepaw glabrous skin and show that the sensory apparatus is highly specialized and more sensitive than the sensory innervation of the mouse hindlimb. This new preparation could be used to examine the impact of genetic mutations that cause sensory abnormalities in man at a mechanistic level. Understanding how injury or disease lead to sensory disorders could be greatly helped by looking at the mouse forepaw, which is, like the human hand, highly specialized for fine tactile discrimination.

Supporting information

Additional supporting information may be found online in the Supporting Information section at the end of the article.

Supplementary Video 1. A series of confocal microscopy images (multiple z-stacks) of one entire footpad showing NF200-positive fibres innervating Meissner's corpuscles.

Supplementary Video 2. The experimental set-up for recording directional sensitivity of glabrous D-hair receptors. The single hairs were moved within a glass capillary and the corresponding single-unit firing behaviour is shown in response to four axes of movement.

Supplementary Video 3. Maximum intensity projection of tdTomato labelled endings around a single glabrous hair follicle.